Preprint Title Potential of deep eutectic solvents in silver nanoparticles fabrication for antibiotic residue detection

Authors Le Hong Tho, Bui Xuan Khuyen, Ngoc Xuan Dat Mai and Nhu Hoa Thi Tran

Publication Date 27 Dez. 2023

Article Type Full Research Paper

ORCID® iDs Ngoc Xuan Dat Mai - https://orcid.org/0000-0001-6752-4173; Nhu Hoa Thi Tran - https://orcid.org/0000-0002-1530-2402

Potential of deep eutectic solvents in silver nanoparticles fabrication for antibiotic residue detection

Le Hong Tho[1,2,3], Bui Xuan Khuyen[4], Ngoc Xuan Dat Mai[2,3], Nhu Hoa Thi Tran[*1,2]

Address:

[1]Faculty of Materials Science and Technology, University of Science, Ho Chi Minh City, Vietnam

[2]Vietnam National University, Ho Chi Minh City, Vietnam

[3]Center for Innovative Materials and Architectures (INOMAR), Ho Chi Minh City, Viet Nam

[4]Institute of Materials Science, Vietnam Academy of Science and Technology, Hanoi, Vietnam

Email:

Nhu Hoa Thi Tran[*] - ttnhoa@hcmus.edu.vn

* Corresponding author

Abstract

Deep eutectic solvents (DESs) have been well-known lately because of their exceptional thermal stability, polarity, and environmental friendliness. There have been numerous advancements in silver nanoparticles (Ag NPs) fabrication, but no attention

to the potential of DES in Ag NPs synthesis is considered and studied carefully. In this study, we present a novel strategy using a selected DES to fabricate Ag NPs in which $AgNO_3$ is chemically reduced by L-ascorbic acid. The results adapted from characterization methods demonstrate that Ag NPs are successfully fabricated, which are further used for the construction of the surface-enhanced Raman scattering (SERS) substrate. The two analytes chosen for SERS quantitation are nitrofurantoin (NFT) and sulfadiazine (SDZ), which throughout the SERS technology, their residues can be traced at 10^{-8} M for both NFT and SDZ. The highest enhancement factors (EFs) are competitive, 6.29×10^{7} and 1.69×10^{7} for NFT and SDZ, respectively. Besides, the linearity coefficients are extremely close to 1 in the range of 10^{-8} M to 10^{-3} M of concentration, and the SERS substrate shows attentional uniformity along with great selectivity. These powerful SERS performances coherently indicate that DESs have tremendous potential in nanomaterials fabrication applied for biosensors' substrate construction.

Keywords

Ag NPs, deep eutectic solvents, potential, antibiotic residue, SERS

Introduction

Surface-enhanced Raman scattering (SERS) is a ubiquitous technology for detecting and tracing substances applied in various kinds of sensors. The spectra as outputs of SERS-based biosensors are simple but powerful results in which every single component of the analytes could be recognized via characteristic vibrations of identical groups [1]. In particular, SERS remains an advantageous and practical choice for biosensors in clinical trials thanks to fast response [2], real-time measurement [3],

extremely high sensitivity improvements [4], attentional selectivity [5], and tremendous versatility [4,6]. Therefore, many scholars have taken advantage of these transcendent properties in cancer diagnosis [7], hazardous chemicals detection [8], concerned microorganisms tracing [9,10], and other analytical measurements applied to food, medical, and environmental issues [11–13]. Undeniably, SERS is the future for comprehensive sensor construction.

Most of SERS's achievements so far rely strictly on the development of plasmonic materials. Noble metals (Au, Ag, Cu…) belong to the most important group of plasmonic materials that extensively respond to electromagnetic waves with proper wavelengths in terms of free electrons oscillation resonating to the incident waves [8,14]. This is the fundamental principle of how surface plasmon resonance (SPR) occurs. Moreover, plasmons are easily controlled at the nanoscales where the particles' shape, size, and surface morphology are various [15]. Deep insight into contact among every adjacent nanoparticle, "hot spots" in which electromagnetic fields are effectively enlarged represents localized surface plasmon resonance (LSPR) [1,16]. Crucial parts of the SERS-based biosensors are commonly composed of LSPR materials [16], which help construct either individual or whole substrates. With the considerable development of synthesis techniques, numerous nanostructures of noble metals have been well-studied to heighten the intrinsic parameters of sensors.

Silver nanoparticles (Ag NPs) have great performance towards sensing applications owing to their highest LSPR properties among the noble metals [17]. One of the decisive factors assisting the SERS performance of Ag NPs-based platforms is the agglomeration state of nanoparticles [18], which directly affects the "hot spots" creation between adjacent particles. There have been many studies in which agglomeration of Ag NPs is adjusted by different kinds of surfactants such as cetyltrimethylammonium bromide (CTAB) [19,20], polyvinylpyrrolidone (PVP) [17], sodium dodecyl sulfate

(SDS), etc [20,21]. However, these chemical substances are the reasons for many negative effects on environmental aspects including microbial, plants, soil, and marine ecosystems as wholly reported by Sharrel Rebello et al [22]. This restricts the applicability of Ag NPs in the biomedical field generally as well as the requirement for eco-friendly available products.

Recently, deep eutectic solvents (DESs) have emerged as a phenomenon in the chemical synthesis of nanomaterials. DESs show superior properties including exclusive thermal stability, impressive polarity, considerably low vapor pressure, and nontoxic essence which make DESs promising candidates for thousands of replacements of industrial solvents [23]. DESs are so versatile that they have been used for nanomaterials synthesis [24]. In the class of plasmonic materials, gold nanoparticles (Au NPs) were first fabricated in DESs [25]. They successfully constructed SERS platforms based on Au NPs-DES whose sensitivity and durability are competitive to the other materials [26,27]. However, there has not been any attention on DESs' potential in Ag NPs fabrication. The similarities between Ag NPs and Au NPs but higher LSPR along with SERS performance of Ag NPs [17,28] lead to the innovative idea of Ag NPs synthesis in DES.

In this work, we present a novel strategy to fabricate Ag NPs as well as demonstrate our hypothesis about the possibility of DES in stabilizing Ag NPs. The product named Ag NPs-DES is used for SERS detection of toxic antibiotics such as nitrofurantoin (NFT) and sulfadiazine (SDZ). These substances have been widely used since the 1970s because of rapid and absolute results on microbials [29], but they are also responsible for hormonal havoc, methemoglobinemia, allergy, damaged liver, nausea, cancers, etc [30–33]. Despite these side effects, they are illegally overused in the food industry and medicine which threatens the human food chain, and negatively affects public health [34]. By evaluating the SERS parameters of Ag NPs-DES substrate on

the NFT and SDZ detection, we propose an applicable aspect of our product, directly showing the great potential of DESs in sensing areas as well as biomedical applications.

Results and Discussion

Formation of Ag NPs-DES

We introduce the protocol summarily presented in **Figure 1**. Every novel synthesis strategy needs to prove the presence of materials. Herein, the UV-vis and XRD are the most straightforward methods that we pick for our hypothesis's evaluation. **Figure 2A** shows the broad adsorption band indicating the high exciton [35] available within dense electron clouds on the surface of Ag NPs due to the SPR phenomenon. Accordingly, the SPR peak is located at 390 nm of wavelength, which is suitable for available SERS applications with laser 532 nm excitation. Besides, the UV-vis spectrum shape is parallel to the Mie scattering theory calculation as reported by theother study [36] proving the existence of Ag NPs in the solution evidently. Moreover, the XRD pattern of the constructed thin film (**Figure 2B**) points out the four characteristic peaks at 38.2°, 44.3°, 64.4°, and 77.6° corresponding to the (111), (200), (220), and (311) planes, respectively. Once the presence of FCC lattice planes characterized by silver element is noted, we claim that Ag NPs-DES is successfully synthesized [37], and the novel procedure is rudimentarily valuable in Ag NPs fabrication.

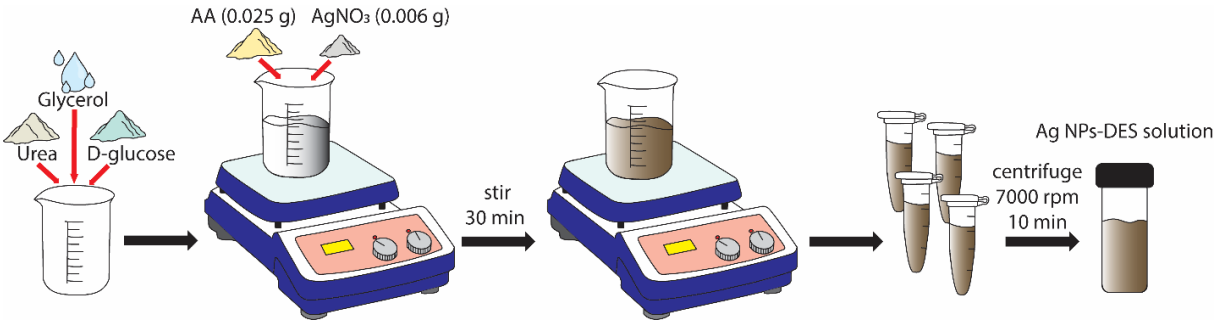

Figure 1. Schematic of Ag NPs-DES synthesizing.

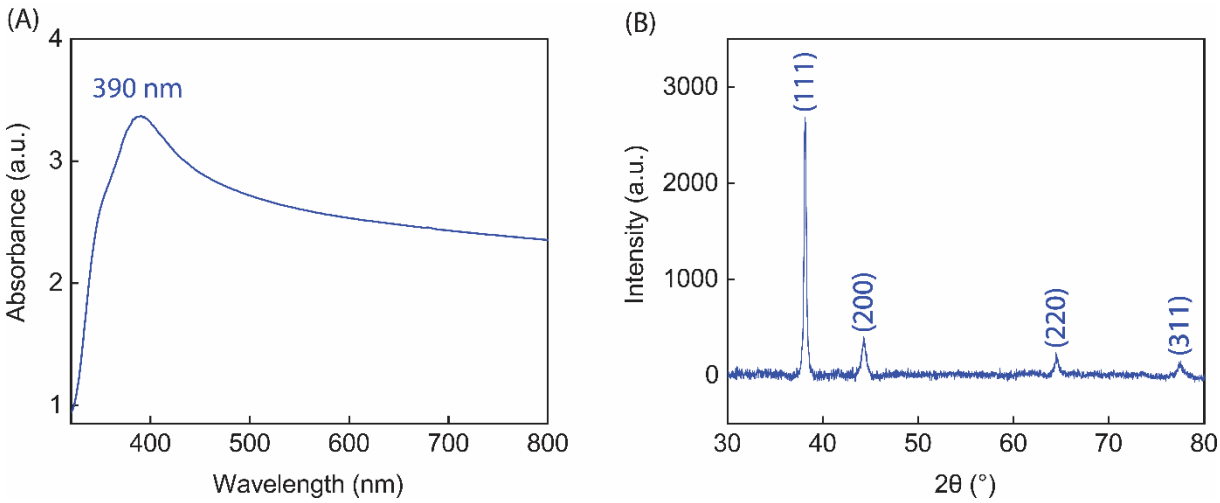

Figure 2. (A) UV-vis spectrum of Ag NPs-DES solution. (B) XRD pattern of Ag NPs-DES thin film.

The development of clusters into nanoparticles following our strategy is supported by DES. DES was reported to be a potential shape-controlling agent, in which highly branched nanostructures were the most common [38]. In our procedure, $AgNO_3$ was added right after AA dissolved well in DES at room temperature. The color of the mixture gradually turned from yellow-orange to dark brown assigned to Ag NPs crystallization. The synthesized Ag NPs-DES is specified by a rod-like shape as well as a high aggregation state (**Figure 3A**). This is because of the extreme viscosity of DES that directly affected the magnetical stirring and tended to form nonspherical shapes of Ag NPs-DES. The aggregated Ag NPs are supported by pure DES in which oxygen and hydrogen atoms of compositional D-glucose, urea, and glycerol tend to form hydrogen bonds. Coherently, this component acts as a surfactant helping to stabilize Ag NPs. Furthermore, the XRF mapping was used to evaluate the presence of silver elements on the thin film. Specifically, the pink dot collective shows the distribution of silver, representing the uniformity of Ag NPs-DES thin film. As observed from **Figure 3B**, there is a consistency in the intensity of pink dots, thus, this clarifies

the high uniformity of Ag NPs-DES coating on the glass substrate, which crucially defines the applicability of this material.

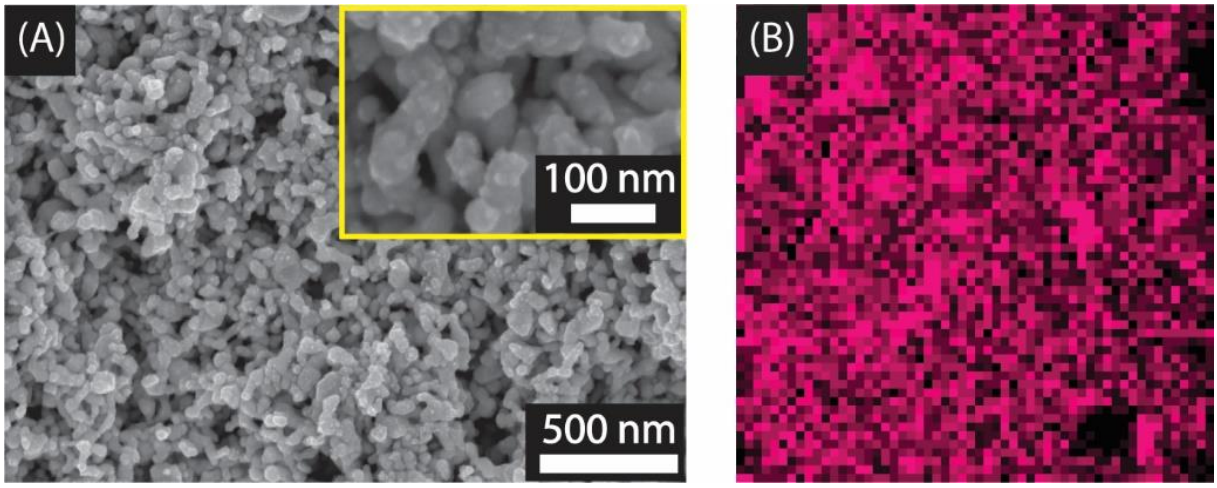

Figure 3. (A) SEM images of Ag NPs-DES. (B) XRF mapping of the Ag NPs-DES thin film in the presence of silver element (pink dots).

NFT detection:

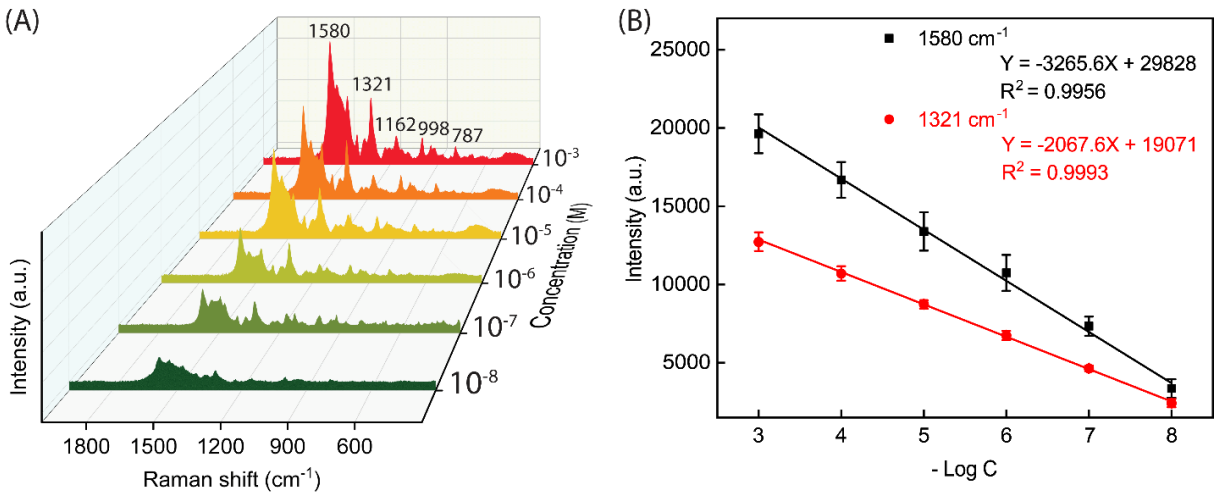

Figure 4. (A) SERS performance of Ag NPs-DES substrate in detecting of different concentrations of NFT. (B) Linear fitting of – Log C and peak intensity at 1580 cm^{-1} and 1321 cm^{-1} (C stands for the concentration of NFT).

Table 1: Vibrational modes assigned to specific peaks in Raman spectra of selected antibiotics.

Chemicals	Frequency (cm^{-1})	Assignment	Ref.
NFT	1580	v N-N=C, v $-NO_2$	[39,40]
	1321	ω N-H	
	1162	ρ (furan ring)	
	998	ρ (hydantoin ring)	
	787	v C-H	
SDZ	1567	ω N-H, v (benzene ring)	[41]
	1356	v C-N	
	1055	v S=O	
	856	τ (pyrimidine ring)	
	610	ω (benzene ring)	

v-streching; ω-bending; τ-torsion; ρ-deformation

The most fundamental component of a SERS-based biosensor is its SERS substrate. It directly affects the SERS performance which coherently helps to evaluate the value of the biosensor [6]. Herein, the Ag NPs-DES thin film with the priority of superior uniform Ag NPs-DES coating can be used as a SERS substrate for antibiotic SERS analysis. Firstly, NFT residue tracing is conducted in the range of 10^{-3} M down to 10^{-8} M concentration (**Figure 4A**). At the limit of detection (LOD) 10^{-8} M, the SERS spectrum clearly shows the emerged peaks in which the highest enhancement factor (EF) reaches 6.29×10^{7}, proving the NFT residue tracing capability of Ag NPs-DES substrate. Furthermore, these peaks correspond to vibrations of characteristic groups of NFT as reported in **Table 1**, notically the most intense ones at 1580 cm^{-1} and 1321 cm^{-1} wavenumbers. Consequently, the two highlighted intensity peaks are solely collected to construct the calibration curves as shown in **Figure 4B**. The reliability values R^2 at 1580 cm^{-1} and 1321 cm^{-1} are 0.9956 and 0.9993, respectively, which are

close to 1 ideally. This indicates that the Ag NPs-DES substrate is sensitive and can be used for quantitative analysis of NFT following the two linear fitting equations:

$$I_{1580} = 3265.6 \log[NFT] + 29828 \quad (1)$$

$$I_{1321} = 2067.6 \log[NFT] + 19071 \quad (2)$$

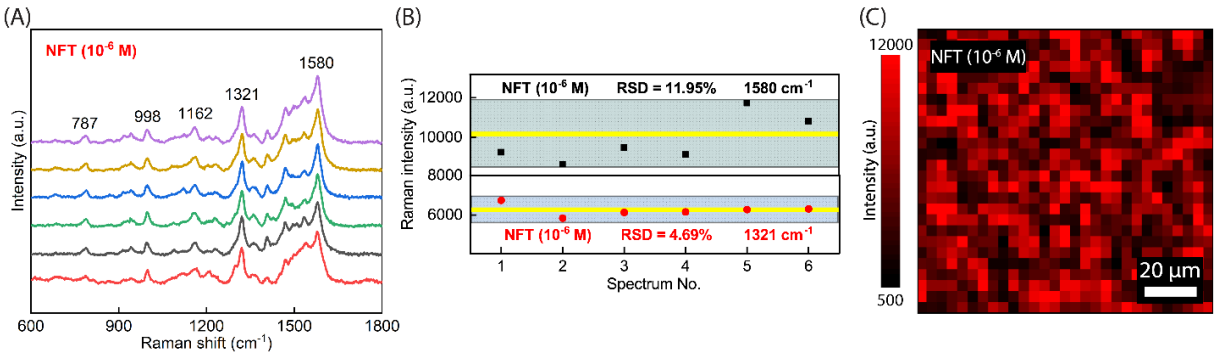

Figure 5. (A) SERS spectra of different chosen points on the Ag NPs-DES substrate. (B) Variation of peak intensity at the two picked-up wavenumbers. (C) SERS mapping of NFT (10^{-6} M) detected on the Ag NPs-DES substrate.

For further investigation on the SERS performance of the Ag NPs-DES thin film, NFT is re-selected to test the stability. In practice, a stable SERS substrate not only is able to withstand the conditions of storage but also has consistency in Raman signals over the surface of the coating. Typically, six different spots on the Ag NPs-DES substrate were pointed out for 10^{-6} M NFT dropping (**Figure 5A**). Then, SERS spectra were analyzed by considering the variation of peak intensity at the two most enhanced Raman shifts 1580 cm^{-1} and 1321 cm^{-1}. In the diagram shown in **Figure 5B**, the yellow lines indicate the average intensity while the areas covering the whole attentional points stand for deviations. Attentionally, these analytical peaks show comparatively low relative standard deviation (RSD): 11.95% at 1580 cm^{-1}, and 4.69% at 1321 cm^{-1}, respectively. In addition, SERS mapping of 10^{-6} M NFT investigated on the substrate also helps to provide a larger scope on the uniformity of SERS signals. As shown in **Figure 5C**, there is plenty of high intensity in the manner of red dots corresponding to

signal enhancement by the Ag NPs-DES substrate, and the highly even distribution assigned to the good uniformity, i.e., satisfactory stability. These results can be explained by the intrinsic LSPR phenomenon of the rod-like Ag NPs synthesized in DES which plays an important role in the high intensity [42] appearing densely in the SERS mapping figure, and the extremely uniform Ag NPs-DES coating barely proven in **Figure 3B**.

SDZ detection and the selectivity of Ag NPs-DES substrate:

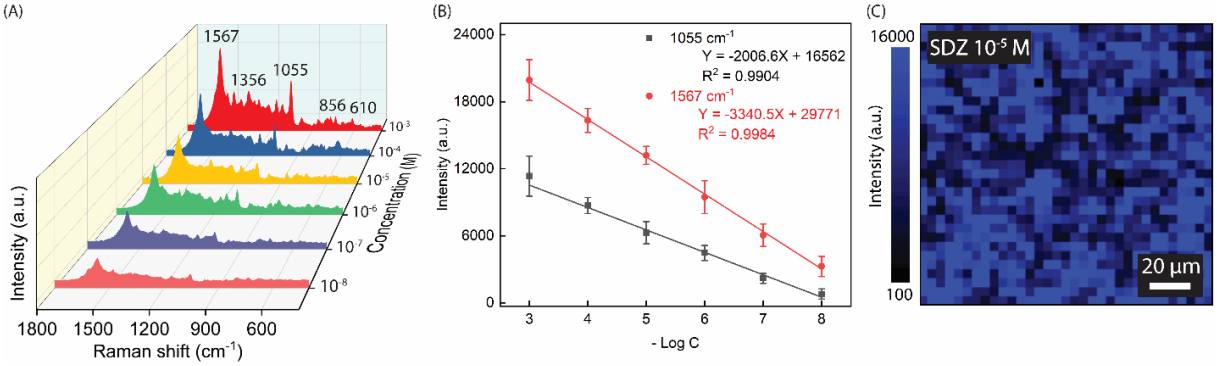

Figure 6. (A) Collection of SERS spectra of SDZ detected in the concentration range 10^{-3} M to 10^{-8} M. (B) Linear fitting between the SDZ concentrations and intensity of the peaks at 1055 cm^{-1} and 1567 cm^{-1}. (C) SERS mapping adapted from the SDZ 10^{-5} M detection on the Ag NPs-DES substrate.

Another antibiotic commonly used in infectious disease treatment is SDZ. Both NFT and SDZ are effective antimicrobial substances, but their overuse statuses were reported to be hazardous as mentioned above. Since their molecular structures are partially different [43,44], SERS analysis is meaningful for the selectivity test of the Ag NPs-DES substrate. As for the procedure of NFT investigations, various concentrations of SDZ were dropped and excited by laser simultaneously (**Figure 6A**) and collected peak intensity data were also used for calibrated curves (**Figure 6B**). The substrate shows linear range from 10^{-3} M to 10^{-8} M, in which the LOD value is 10^{-8} M, and the highest EF reaches 1.69×10^{7}. The vibration modes of assigned peaks are listed in

Table 1. Additionally, there are two peaks clearly enhanced at 1567 cm^{-1} and 1055 cm^{-1} whose correlation factors R^2 equal 0.9984 and 0.9904, respectively. Along with parameters of NFT SERS analysis constructed previously, these high R^2 values help to provide undeniable proof of the remarkable quantity ability of our Ag NPs-DES substrate on antibiotic residue tracing. The linear regressions of the two chosen analytical peaks of SDZ are presented as follows:

$$I_{1567} = 3340.5 \log[SDZ] + 29771 \quad (3)$$

$$I_{1055} = 2006.6 \log[SDZ] + 16562 \quad (4)$$

Although the consistency in SERS signals recorded on the Ag NPs-DES substrate has been investigated with NFT 10^{-6} M, we need to evaluate the SERS mapping image of SDZ to ensure the stability of our substrate with the change of analytes. Therein, 10^{-5} M of SDZ was dropwise and let dry naturally before the laser excitation. SERS mapping shown in **Figure 6C** clarifies the dense responses to electromagnetic waves correspond to an even distribution of high intensity over the entire considered surface. This coherently claims that the Ag NPs-DES coating has good consistency despite the various selection of analytes. Attentionally, DES is supposed to play a crucial role in helping to disperse Ag NPs suspension via its hydrogen bonding networks [26], which accurately accumulate the linkage formation possibility between $-NH_2$ groups of APTES and Ag NPs. This eventually explains the steady evenness of Ag NPs-DES thin film.

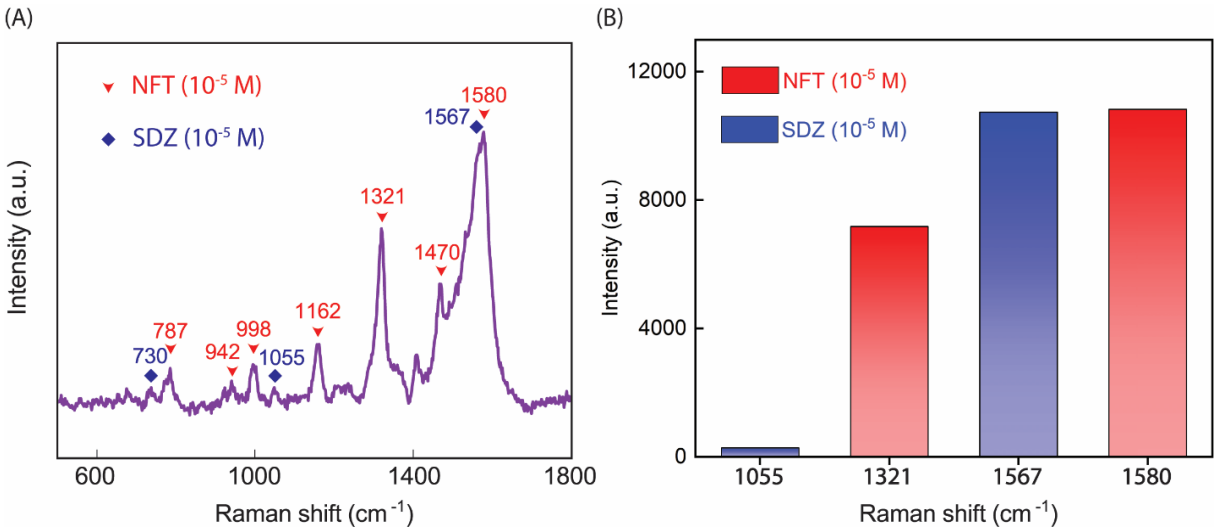

Figure 7. (A) SERS spectrum of NFT (10^{-5} M) and SDZ (10^{-5} M) solution. (B) Specific peak intensity identification corresponding to NFT and SDZ.

Another type of selectivity test was carried out with a solution containing 10^{-5} M NFT and 10^{-5} M SDZ. The SERS spectrum in **Figure 7A** verifies the difference in Raman shifts among the characteristic peaks of the two analytes. Here, the blue diamonds represent SDZ's key peaks, whereas the red arrows stand for NFT's ones. With the presence of all characteristic peaks, NFT is effortless to detect in the solution thanks to the exclusive intensity. In contrast, compositional SDZ's SERS spectrum shows solely three peaks instead of five ones in common. Additionally, the two most intense peaks of both NFT at 1580 cm^{-1} and SDZ at 1567 cm^{-1} overlap which makes it difficult to ascertain intensity for quantitative determinations (**Figure 7B**). Therefore, we propose peaks at 1321 cm^{-1} of NFT and 1055 cm^{-1} of SDZ as alternatives. Their intensity is comparable to the base of the SERS spectrum, and they are separated from each other as well as the others. Based on the data experimentally collected and the correlation between – Log C and peak intensity as followed equations (2) and (4), NFT and SDZ can be determined concentrations desperately. This surely can be applied to another solution of various substances, indicating that Ag NPs-DES substrate has good quality of selectivity. Moreover, compared to other studies on NFT

and SDZ detection (**Table 2**), Ag NPs-DES material shows competative LOD values and linear range. Thus, Ag NPs-DES is a promising candidate in SERS applications along with the tremendous potential of DES in Ag NPs fabrication.

Table 2: An overview of reported studies on NFT and SDZ detection.

Analytes	Materials	Year	LOD	Linear range	Ref.
NFT	Au NPs/GO	2021	5 ng/mL	5 – 500 ng/mL	[45]
	BT/CNF/GCE	2021	0.005 μM	0.06 – 450 μM	[46]
	N-CQD@Co_3O_4/MWCNT	2020	0.044 μM	0.05 – 1220 μM	[47]
	NiO/BCN	2019	10 nM	0.05 – 230 μM	[48]
	Ag NPs-DES	**2023**	**10^{-8} M**	**10^{-3} – 10^{-8} M**	**This work**
SDZ	$SrWO_4$	2021	0.009 μM	0.05 – 235 μM	[49]
	Au NPs	2021	1 μg/L	1 – 100 μg/L	[44]
	RGO/Ag - coated alloy fiber	2019	1.9 ng/cm^3	0.01 – 100 μg/cm^3	[50]
	MIP - QDs	2019	0.67 μM	4 – 20 μM	[51]
	Ag NPs-DES	**2023**	**10^{-8} M**	**10^{-3} – 10^{-8} M**	**This work**

Conclusion

In this study, we have proposed a novel strategy for Ag NP synthesis in DES. The Ag NPs-DES sample was prepared successfully with the chemical reduction in which DES acts as either a solvent or a shape-controlling agent. Our rapid, low-cost procedure does not require any other toxic substances, elucidating its efficiency appropriate for

the eco-friendly synthesis trend. Using NFT and SDZ as probe molecules, the SERS performance of Ag NPs-DES was discussed in which the LOD value is 10^{-8} M in NFT and SDZ detections. The EF values are relatively high, 6.29×10^{7} for NFT and 1.69×10^{7} for SDZ, and linearity coefficients are extremely close to 1, proving the quantitative tracing residue capabilities of the synthesized Ag NPs-DES substrate. Besides sensitivity, uniformity of the coating, consistency in SERS signals, and selectivity also show outstanding results. Overall, Ag NPs-DES is a promising candidate for SERS-based biosensor applications, whose DES successfully shows its productive favorable characteristics. This work hopefully provides useful information about DES's potential in nanomaterials fabrication and possible guidance for low-cost as well as effective SERS substrate construction in biosensors.

Experimental

Chemicals:

L-ascorbic acid (AA, $C_6H_8O_6$, 99%), silver nitrate ($AgNO_3$, 99%), (3-Aminopropyl)triethoxysilane (APTES, 99%), NFT ($C_8H_6N_4O_5$, 98%), and SDZ ($C_{10}H_{10}N_4O_2S$, 99%) were purchased from Sigma-Aldrich Co., MO, USA. Urea (CH_4N_2O, 99%) was obtained from ACS, Reag. Ph Eur, Merck Co., Germany whereas glycerol ($C_3H_8O_3$, 99%) was supplied by Daejung Ltd., Korea. D-glucose ($C_6H_{12}O_6$, 99%) was purchased from Fisher Ltd., UK. The microscope glass slides (SiO_2, Na_2O, CaO, and MgO) were manufactured by ISOLAB Laborgeräte GmbH, Eschau, Germany.

Fabrication of DES and Ag NPs-DES:

The most ubiquitous DES studied vastly in recent years is reline composed of urea and choline chloride with a 2:1 molar ratio respectively [23]. However, this substance is not

appropriate for Ag NPs synthesis owing to the Cl^- anion being presented in choline chloride, which may unintentionally cause AgCl precipitation. Here, we chose an alternative DES [52] whose compositions did not contain any anions precipitating with Ag^+ cations. D-glucose, urea, and glycerol (molar ratio 1:1:2) were mixed and magnetically stirred at relatively high temperature until a homogenous liquid formed. Then, the mixture was cooled down gradually to room temperature while keeping the vigorous stirring. 0.025 grams of AA was dissolved in 10.195 grams of synthesized DES, and 0.006 grams of $AgNO_3$ was added later which helped the reaction occur. After 30 minutes of constant stirring, the obtained Ag NPs-DES were washed with DI water several times, and the pellets were redispersed in DI water for further use.

The Ag NPs-DES thin film was prepared following the procedure for self-assembly monolayer (SAM) construction. A clean glass substrate was treated with oxygen plasma to form the reactive -OH group on the surface. The substrate was then soaked in the 3% ethanolic solution of APTES for 2 hours which helped to stabilize the $-NH_2$ group. A total of 2 mL of Ag NPs-DES solution was used to deposit Ag NPs on the glass substrate via Ag – NH_2 linkage by fully immersing the treated glass for 2 hours. At last, the product was dried naturally at room temperature, resulting in the successful fabrication of Ag NPs-DES substrate.

NFT and SDZ detection on the Ag NPs-DES substrate:

Various concentrations from 10^{-3} M to 10^{-8} M of NFT and SDZ were dropwise on the Ag NPs-DES substrate in the amount of 20 µL for each measurement. The analyte was then dried at room temperature and recorded Raman spectra instantaneously via laser 532 nm excitation. Other investigations on the SERS performance of our sample were also carried out as following these steps including Raman mapping, signal consistency, uniformity, and selectivity.

Instrument characterization and apparatus:

The absorbance properties of the sample were recorded via a V−730 visible/NIR machine supplied by JASCO, Japan. The crystallinity of the Ag NPs-DES thin film was tested by a D8 advance diffractometer, Bruker, UK with a Ni-fillter Cu Kα X-ray source. To evaluate the nanostructure and surface morphology of nanoparticles, as well as the elemental distribution of silver on the substrate, S4800 filed-emission scanning electron microscopy (SEM) purchased from Hitachi, Japan, and M4 TORNADO^{Plus} Micro X-ray fluorescence Spectrometer with a Rh tube at 30 W micro-focus light element of Bruker, UK. Raman spectra were collected from XploRA ONE spectroscopy, HORIBA, Japan, in which the laser was specified by wavelength of 532 nm, 1 mW power, and 60 accumulations time.

Acknowledgements

This research is funded by University of Science, VNU-HCM under grant number T2023-149.

Declarations

Conflict of interest

The authors declare that they have no known competing financial interests or personal relationships that could have appeared to influence the work reported in this paper.

References

1. Alvarez-Puebla, R. A.; Liz-Marzán, L. M. *Small* **2010**, *6*, 604–610. doi:10.1002/SMLL.200901820
2. Zhao, B.; Yang, T.; Qu, Y.; Mills, A. J.; Zhang, G.; He, L. *Science of the Total Environment* **2020**, *716*. doi:10.1016/j.scitotenv.2020.137097

3. Liu, J.; Zheng, T.; Tian, Y. *Angewandte Chemie International Edition* **2019**, *58*, 7757–7761. doi:10.1002/ANIE.201902776

4. Arabi, M.; Ostovan, A.; Wang, Y.; Mei, R.; Fu, L.; Li, J.; Wang, X.; Chen, L. *Nat Commun* **2022**, *13*. doi:10.1038/s41467-022-33448-w

5. Lin, D.; Dong, R.; Li, P.; Li, S.; Ge, M.; Zhang, Y.; Yang, L.; Xu, W. *Talanta* **2020**, *218*. doi:10.1016/j.talanta.2020.121157

6. Liang, X.; Li, N.; Zhang, R.; Yin, P.; Zhang, C.; Yang, N.; Liang, K.; Kong, B. Carbon-Based SERS Biosensor: From Substrate Design to Sensing and Bioapplication. *NPG Asia Materials*. Nature Research December 1, 2021. doi:10.1038/s41427-020-00278-5

7. Li, L.; Jiang, R.; Shan, B.; Lu, Y.; Zheng, C.; Li, M. *Nat Commun* **2022**, *13*. doi:10.1038/s41467-022-32975-w

8. La Ngoc Tran, N.; Van Hoang, D.; Tuan Thanh Pham, A.; Tran Truc Phuong, N.; Xuan Dat Mai, N.; Chi, T. T. K.; Hien, B. T. T.; Bach Phan, T.; Tran, N. H. T. *Journal of Science: Advanced Materials and Devices* **2023**, *8*. doi:10.1016/j.jsamd.2023.100584

9. Eskandari, V.; Sahbafar, H.; Zeinalizad, L.; Hadi, A. *ISSS J Micro Smart Syst* **2022**, *11*, 363–382. doi:10.1007/s41683-022-00103-x

10. Xia, J.; Li, W.; Sun, M.; Wang, H. *Nanomaterials 2022, Vol. 12, Page 3572* **2022**, *12*, 3572. doi:10.3390/NANO12203572

11. Lin, D. Y.; Yu, C. Y.; Ku, C. A.; Chung, C. K. *Micromachines 2023, Vol. 14, Page 1343* **2023**, *14*, 1343. doi:10.3390/MI14071343

12. Schlücker, S. SERS Microscopy: Nanoparticle Probes and Biomedical Applications. *ChemPhysChem*. Wiley-VCH Verlag July 13, 2009, pp 1344–1354. doi:10.1002/cphc.200900119

13. Nguyen, D. K.; Dinh, V. P.; Dang, N. T.; Khan, D. T.; Hung, N. T.; Thi Tran, N. H. *RSC Adv* **2023**, *13*, 20565–20574. doi:10.1039/d3ra02552g

14. Chegel, V. I.; Lopatynskyi, A. M. *Molecular Plasmonics; Theory and Applications*

15. Nickelson, L. *Electromagnetic Theory and Plasmonics for Engineers*; Springer Singapore, 2018. doi:10.1007/978-981-13-2352-2

16. Xu, T.; Geng, Z. Strategies to Improve Performances of LSPR Biosensing: Structure, Materials, and Interface Modification. *Biosensors and Bioelectronics*. Elsevier Ltd February 15, 2021. doi:10.1016/j.bios.2020.112850

17. Truc Phuong, N. T.; Dang, V. Q.; Van Hieu, L.; Bach, T. N.; Khuyen, B. X.; Thi Ta, H. K.; Ju, H.; Phan, B. T.; Thi Tran, N. H. *RSC Adv* **2022**, *12*, 31352–31362. doi:10.1039/d2ra06074d

18. Zook, J. M.; Rastogi, V.; MacCuspie, R. I.; Keene, A. M.; Fagan, J. *ACS Nano* **2011**, *5*, 8070–8079. doi:10.1021/nn202645b

19. Iqbal, N.; Iqubal, S. M. S.; Khan, A. A.; Mohammed, T.; Alshabi, A. M.; Aazam, E. S.; Rafiquee, M. Z. A. *J Mol Liq* **2021**, *329*. doi:10.1016/j.molliq.2021.115537

20. AL-Thabaiti, S. A.; Al-Nowaiser, F. M.; Obaid, A. Y.; Al-Youbi, A. O.; Khan, Z. *Colloids Surf B Biointerfaces* **2008**, *67*, 230–237. doi:10.1016/j.colsurfb.2008.08.022

21. Naseem, K.; Ali, F.; Tahir, M. H.; Afaq, M.; Yasir, H. M.; Ahmed, K.; Aljuwayid, A. muteb; Habila, M. A. *J Mol Struct* **2022**, *1262*, 132996. doi:10.1016/J.MOLSTRUC.2022.132996

22. Rebello, S.; Asok, A. K.; Mundayoor, S.; Jisha, M. S. Surfactants: Toxicity, Remediation and Green Surfactants. *Environmental Chemistry Letters*. Springer Verlag 2014, pp 275–287. doi:10.1007/s10311-014-0466-2

23. Smith, E. L.; Abbott, A. P.; Ryder, K. S. Deep Eutectic Solvents (DESs) and Their Applications. *Chemical Reviews*. American Chemical Society November 12, 2014, pp 11060–11082. doi:10.1021/cr300162p

24. Abo-Hamad, A.; Hayyan, M.; AlSaadi, M. A. H.; Hashim, M. A. Potential Applications of Deep Eutectic Solvents in Nanotechnology. *Chemical Engineering Journal*. Elsevier B.V. August 1, 2015, pp 551–567. doi:10.1016/j.cej.2015.03.091

25. Liao, H. G.; Jiang, Y. X.; Zhou, Z. Y.; Chen, S. P.; Sun, S. G. *Angewandte Chemie International Edition* **2008**, *47*, 9100–9103. doi:10.1002/ANIE.200803202

26. Mahyari, F. A.; Tohidi, M.; Safavi, A. *Mater Res Express* **2016**, *3*. doi:10.1088/2053-1591/3/9/095006

27. Raghuwanshi, V. S.; Ochmann, M.; Hoell, A.; Polzer, F.; Rademann, K. *Langmuir* **2014**, *30*, 6038–6046. doi:10.1021/LA500979P/SUPPL_FILE/LA500979P_SI_001.PDF

28. Lismont, M.; Dreesen, L. *Materials Science and Engineering C* **2012**, *32*, 1437–1442. doi:10.1016/j.msec.2012.04.023

29. Zhang, Y.; Yu, Z.; Yue, Z.; Gao, J.; Wu, S.; Zhang, Z.; Li, G. *Journal of Raman Spectroscopy* **2019**, *50*, 1094–1102. doi:10.1002/jrs.5636

30. Kabbara, W. K.; Kordahi, M. C. Nitrofurantoin-Induced Pulmonary Toxicity: A Case Report and Review of the Literature. *Journal of Infection and Public Health*. Elsevier Ltd July 1, 2015, pp 309–313. doi:10.1016/j.jiph.2015.01.007

31. Lewkowski, J.; Rogacz, D.; Rychter, P. *Chemosphere* **2019**, *222*, 381–390. doi:10.1016/j.chemosphere.2019.01.144

32. Mariyappan, V.; Keerthi, M.; Chen, S. M.; Jeyapragasam, T. *J Colloid Interface Sci* **2021**, *600*, 537–549. doi:10.1016/j.jcis.2021.05.035

33. Wu, W.; Mehedi Hassan, M.; Ding, X.; Wu, J.; Ouyang, Q.; Chen, Q. *Microchemical Journal* **2023**, *191*. doi:10.1016/j.microc.2023.108765

34. Ezhil Vilian, A. T.; Hwang, S. K.; Bhaskaran, G.; Alhammadi, M.; Kim, S.; Tiwari, J. N.; Suk Huh, Y.; Han, Y. K. *Chemical Engineering Journal* **2023**, *454*. doi:10.1016/j.cej.2022.139980

35. Hou, Y.; Zhang, W.; Li, S.; Wang, Z.; Zhong, H.; Liu, Z.; Guo, Z. *Analyst* **2018**, *143*, 3677–3685. doi:10.1039/c8an00405f

36. Perkampus, H.-H. *UV-VIS Spectroscopy and Its Applications*; Springer Berlin Heidelberg, 1992. doi:10.1007/978-3-642-77477-5

37. Tran Truc Phuong, N.; Xoan Hoang, T.; La Ngoc Tran, N.; Gia Phuc, L.; Phung, V. D.; Kieu Thi Ta, H.; Ngoc Bach, T.; Hoa Thi Tran, N.; The Loan Trinh, K. *Spectrochim Acta A Mol Biomol Spectrosc* **2021**, *263*. doi:10.1016/j.saa.2021.120179

38. Mahyari, F. A.; Tohidi, M.; Safavi, A. *Mater Res Express* **2016**, *3*. doi:10.1088/2053-1591/3/9/095006

39. Wang, Y.; Chen, H.; Jiang, L. *Analyst* **2021**, *146*, 5740–5746. doi:10.1039/d1an01185e

40. Chen, J.; Li, S.; Yao, F.; Xu, W.; Li, Y.; Chen, Q.; Liang, P. *Chemosensors* **2023**, *11*. doi:10.3390/chemosensors11040232

41. Shen, X. R.; Zheng, H.; Pang, R.; Liu, G. K.; Wu, D. Y.; Tian, Z. Q. *Journal of Physical Chemistry A* **2019**, *123*, 9199–9208. doi:10.1021/acs.jpca.9b07346

42. Francis, M. K.; Sahu, B. K.; Bhargav, P. B.; C, B.; Ahmed, N.; Das, A.; Dhara, S. *Physica E Low Dimens Syst Nanostruct* **2022**, *137*, 115080. doi:10.1016/J.PHYSE.2021.115080

43. Mariyappan, V.; Keerthi, M.; Chen, S. M.; Jeyapragasam, T. *J Colloid Interface Sci* **2021**, *600*, 537–549. doi:10.1016/j.jcis.2021.05.035

44. Zhou, Z. M.; Zheng, H.; Liu, T.; Xie, Z. Z.; Luo, S. H.; Chen, G. Y.; Tian, Z. Q.; Liu, G. K. *Anal Chem* **2021**, *93*, 8603–8612. doi:10.1021/acs.analchem.1c01530

45. Wang, Y.; Chen, H.; Jiang, L. *Analyst* **2021**, *146*, 5740–5746. doi:10.1039/d1an01185e

46. Nataraj, N.; Chen, S. M. *Journal of Electroanalytical Chemistry* **2021**, *887*. doi:10.1016/j.jelechem.2021.115152

47. Muthusankar, G.; Devi, R. K.; Gopu, G. *Biosens Bioelectron* **2020**, *150*, 111947. doi:10.1016/J.BIOS.2019.111947

48. Kokulnathan, T.; Wang, T. J. *Compos B Eng* **2019**, *174*. doi:10.1016/j.compositesb.2019.106914

49. Kokulnathan, T.; Kumar, E. A.; Wang, T. J.; Cheng, I. C. *Ecotoxicol Environ Saf* **2021**, *208*, 111516. doi:10.1016/J.ECOENV.2020.111516

50. Cui, J.; Chen, S.; Ma, X.; Shao, H.; Zhan, J. *Microchimica Acta* **2019**, *186*. doi:10.1007/s00604-018-3105-y

51. Shi, T.; Tan, L.; Fu, H.; Wang, J. *Mar Pollut Bull* **2019**, *146*, 591–597. doi:10.1016/j.marpolbul.2019.07.010

52. Zdanowicz, M. *Int J Biol Macromol* **2021**, *176*, 387–393. doi:10.1016/j.ijbiomac.2021.02.039